BRIEF REPORTS

Brief Reports are short papers which report on completed research or are addenda to papers previously published in the **Physical Review.** *A Brief Report may be no longer than four printed pages and must be accompanied by an abstract.*

Deformed negative-parity excitations in ^{71}As

N. Fotiades,[1] J. A. Cizewski,[1,2] C. J. Lister,[2] C. N. Davids,[2] R. V. F. Janssens,[2] D. Seweryniak,[2] M. P. Carpenter,[2] T. L. Khoo,[2] T. Lauritsen,[2] D. Nisius,[2] P. Reiter,[2] J. Uusitalo,[2] I. Wiedenhöver,[2] A. O. Macchiavelli,[3] and R. W. MacLeod[4]

[1]*Department of Physics and Astronomy, Rutgers University, New Brunswick, New Jersey 08903*

[2]*Physics Division, Argonne National Laboratory, Argonne, Illinois 60439*

[3]*Nuclear Science Division, Lawrence Berkeley National Laboratory, Berkeley, California 94720*

[4]*Thomas Jefferson National Laboratory, Newport News, Virginia 23606*

(Received 30 November 1998)

High-spin states in the neutron-deficient ^{71}As nucleus have been studied using in-beam γ-ray spectroscopic techniques combined with mass identification. A new decay sequence of negative parity has been assigned to ^{71}As and previously known sequences have been extended to higher spin and excitation. The new sequence has been identified as originating from the proton $f_{7/2}$ extruder orbital, which approaches the Fermi surface at large prolate deformations. Comparisons of experimental $B(M1)/B(E2)$ ratios to theoretical expectations support this interpretation. [S0556-2813(99)04005-4]

PACS number(s): 23.20.Lv, 27.50.+e

The nuclei in the $A=70$ mass region exhibit a complicated interplay of single-particle and collective degrees of freedom, reflecting the influence of competing shell gaps in the Nilsson single-particle levels. As a result, different deformations occur in the same nucleus, as first observed in this mass region in ^{72}Se [1]. The same interplay is expected to be present in the isotone ^{71}As. Indeed, recent experimental studies [2] of this isotope support the coexistence of triaxial collective and spherical single-particle states, and the conclusions are supported by theoretical calculations of the total Routhian surface (TRS) [2,3]. The calculations for the negative-parity states predict shallow minima at prolate and noncollective oblate deformations at low rotational frequencies, which become more deformed as a function of frequency and triaxial above $\hbar\omega=0.5$ MeV. At large deformations, the prolate minima in the energy surfaces could allow the proton $f_{7/2}$ extruder orbital to come sufficiently close to the Fermi surface to be populated in a heavy-ion induced reaction. This orbital is also critical in the development of deformed and superdeformed shapes in $A=60$ nuclei [4].

High-spin states in ^{71}As have been investigated using the ^{16}O+^{58}Ni reaction at a beam energy of 59.5 MeV. The ^{16}O beam from the ATLAS accelerator at Argonne National Laboratory bombarded a self-supporting 484 μg/cm^2 foil of ^{58}Ni. γ rays at the target position were detected by the Gammasphere array [5] which was coupled to the Fragment Mass Analyzer [6] in order to separate evaporation residues from other reaction products and from scattered beam. This was the first experiment with this setup. γ-γ coincidence events, as well as γ-recoil mass coincidences, have been established. A total γ-γ coincidence matrix, as well as several γ-γ matrices gated on the mass of the recoils, were constructed. Measurements of the directional correlations of the transitions (DCO ratios) have provided the basis for angular momentum and parity assignments for most of the transitions observed. Approximately 6.3 million γ-γ coincidence events were recorded in coincidence with a recoil. Mass 71 and 72 were the strongest channels in this reaction. In addition to the $3p$, ^{71}As reaction channel, ^{68}Ge $(2p\alpha)$, ^{71}Se $(2pn)$, ^{72}Se $(2p)$, and ^{72}Br (pn) have also been identified in this data set. A preliminary report of this work was presented in Ref. [7].

The present study confirms the positive-parity part of the ^{71}As level scheme as reported in Ref. [2]. The partial level scheme of the negative-parity states of ^{71}As obtained in the present work is shown in Fig. 1. The placement of the transitions is based primarily on the coincidence relations between these transitions, their relative intensities, and excitation energy sums. A summary of the experimental information deduced for the transitions in Fig. 1 is given in Table I. Typical values of DCO ratios for stretched dipole and quadrupole transitions are, respectively, 0.5 and 1.0, when gated on a stretched quadrupole transition and, respectively, 1.0 and 2.0, when gated on a stretched dipole transition.

The previously known negative-parity band 1 [2] in Fig. 1 has been extended up to $\sim$10 MeV in excitation energy and the decay of this band towards the lower-lying negative parity states has been confirmed. Previously established [2] transitions to the positive-parity band have been confirmed but are not displayed in Fig. 1. This separation of the negative- and positive-parity portions of the level scheme is appropriate since, for the most part, the deexcitations of the negative- and positive-parity states preserve the parity. The exceptions are a few transitions in the signature $\alpha=-1/2$ partner of band 1 which also feed the positive-parity cascade, as displayed in Fig. 5 of Ref. [2] and as confirmed in the present work. The DCO values for the members of negative-parity

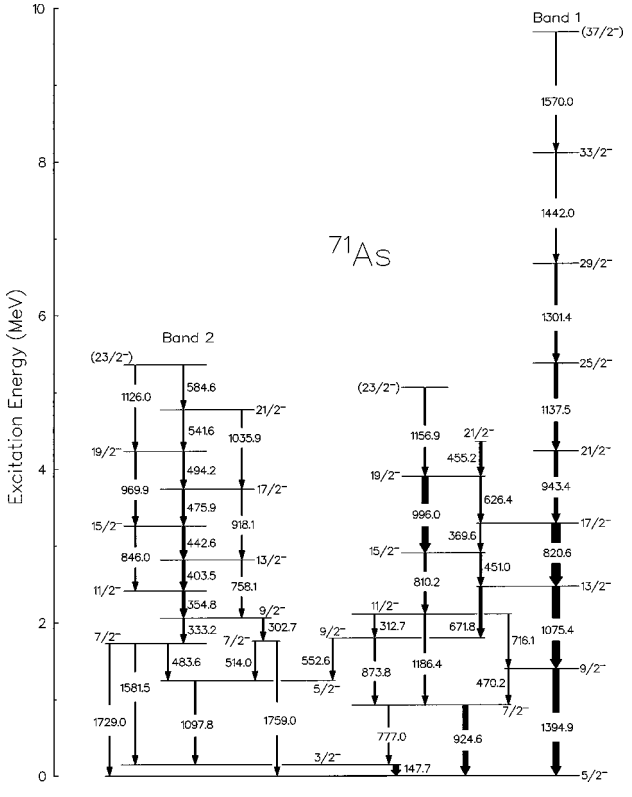

FIG. 1. Partial level scheme of ^{71}As obtained in the present work. Only the states with negative parity are displayed. The width of the arrows is proportional to the intensity of the transitions. The γ-ray energies are in keV.

band 1 support the spin-parity assignments up to the $33/2^-$ state. The 671.8-keV transition ($13/2^- \rightarrow 9/2^-$) could also be regarded as part of the band and it has been included in the calculations below. However, the bulk of the intensity out of the $13/2^-$ state is carried away by the 1075.4-keV transition towards the lower-lying $9/2^-$ state at an excitation energy of 1394.9 keV.

Band 2 in Fig. 1 is a new sequence of negative-parity levels observed at moderate excitations. The spectrum in Fig. 2 is a sum of gates on several band-2 transitions from a matrix gated on $A=71$. The band consists of dipole transitions which compete favorably with quadrupole crossover transitions. The DCO values in Table I support these assignments. Since band 2 only populates the lower-lying negative-parity states and the positive- and negative-parity cascades are essentially decoupled, negative-parity has been assumed for band 2. This band is regular and attains the maximum of its intensity ($\sim$20%) at spin $11/2^-$. At higher excitations, the intensity drops gradually until the band disappears at spin $23/2^-$ and $\hbar\omega \sim 525$ keV.

Due to its rotationlike properties, band 1 has been analyzed extensively in the framework of the cranked shell model in Ref. [2]. The extension of this band to higher excitations in the present work confirms the persistence of these properties at high spins. The kinematic $J^{(1)}$ and dynamic $J^{(2)}$ moments of inertia for this band are shown in Fig. 3. The onset of collectivity occurs at a rotational frequency of $\sim$0.32 MeV and persists up to $\sim$0.8 MeV, with both moments of inertia gradually increasing. The small kink in the dynamical moment of inertia at $\sim$0.42 MeV could be a

TABLE I. Energies, intensities, DCO ratios, and placements of transitions in ^{71}As displayed in Fig. 1. DCO values marked with an asterisk were obtained by gating on a $\Delta I=1$ dipole transition.

Energy[a] (keV)	Intensity[b] (‰)	DCO	Excitation[c] E_i (keV)	E_f (keV)	Assignment I_i^π	$\mapsto$	I_f^π
147.7	277(40)	0.83(7)*	147.7	0.0	$\frac{3}{2}^-$	$\mapsto$	$\frac{5}{2}^-$
302.7	49(10)	1.06(11)*	2062.2	1759.4	$\frac{9}{2}^-$	$\mapsto$	$\frac{7}{2}^-$
312.7	12(4)	0.52(8)	2111.0	1798.4	$\frac{11}{2}^-$	$\mapsto$	$\frac{9}{2}^-$
333.2	79(15)	1.02(6)*	2062.2	1729.0	$\frac{9}{2}^-$	$\mapsto$	$\frac{7}{2}^-$
354.8	141(20)	1.18(9)*	2417.0	2062.2	$\frac{11}{2}^-$	$\mapsto$	$\frac{9}{2}^-$
369.6	30(6)	0.40(12)	3290.9	2921.2	$\frac{17}{2}^-$	$\mapsto$	$\frac{15}{2}^-$
403.5	145(25)	1.09(6)*	2820.5	2417.0	$\frac{13}{2}^-$	$\mapsto$	$\frac{11}{2}^-$
442.6	154(25)	0.90(6)*	3263.1	2820.5	$\frac{15}{2}^-$	$\mapsto$	$\frac{13}{2}^-$
451.0	109(20)	0.59(9)	2921.2	2470.3	$\frac{15}{2}^-$	$\mapsto$	$\frac{13}{2}^-$
455.2	129(30)	0.43(6)	4372.4	3917.2	$\frac{21}{2}^-$	$\mapsto$	$\frac{19}{2}^-$
470.2	30(5)		1394.9	924.6	$\frac{9}{2}^-$	$\mapsto$	$\frac{7}{2}^-$
475.9	102(15)	0.93(9)*	3739.0	3263.1	$\frac{17}{2}^-$	$\mapsto$	$\frac{15}{2}^-$
483.6	15(3)	0.70(10)*	1729.0	1245.5	$\frac{7}{2}^-$	$\mapsto$	$\frac{5}{2}^-$
494.2	81(10)	0.94(9)*	4233.2	3739.0	$\frac{19}{2}^-$	$\mapsto$	$\frac{17}{2}^-$
514.0	26(7)		1759.4	1245.5	$\frac{7}{2}^-$	$\mapsto$	$\frac{5}{2}^-$
541.6	31(6)	1.03(24)*	4774.8	4233.2	$\frac{21}{2}^-$	$\mapsto$	$\frac{19}{2}^-$
552.6	35(8)	0.75(7)	1798.4	1245.5	$\frac{9}{2}^-$	$\mapsto$	$\frac{5}{2}^-$
584.6	6(2)		5359.4	4774.8	$\frac{23}{2}^-$	$\mapsto$	$\frac{21}{2}^-$
626.4	86(10)	0.48(4)	3917.2	3290.9	$\frac{19}{2}^-$	$\mapsto$	$\frac{17}{2}^-$
671.8	149(30)	0.99(7)	2470.3	1798.4	$\frac{13}{2}^-$	$\mapsto$	$\frac{9}{2}^-$
716.1	30(10)		2111.0	1394.9	$\frac{11}{2}^-$	$\mapsto$	$\frac{9}{2}^-$
758.1	40(8)	1.61(31)*	2820.5	2062.2	$\frac{13}{2}^-$	$\mapsto$	$\frac{9}{2}^-$
777.0	33(9)		924.6	147.7	$\frac{7}{2}^-$	$\mapsto$	$\frac{3}{2}^-$
810.2	119(25)	0.89(10)	2921.2	2111.0	$\frac{15}{2}^-$	$\mapsto$	$\frac{11}{2}^-$
846.0	58(10)		3263.1	2417.0	$\frac{15}{2}^-$	$\mapsto$	$\frac{11}{2}^-$
873.8	75(10)		1798.4	924.6	$\frac{9}{2}^-$	$\mapsto$	$\frac{7}{2}^-$
820.6	471(60)	1.02(8)	3290.9	2470.3	$\frac{17}{2}^-$	$\mapsto$	$\frac{13}{2}^-$
918.1	42(5)	2.58(54)*	3739.0	2820.5	$\frac{17}{2}^-$	$\mapsto$	$\frac{13}{2}^-$
924.6	270(50)	0.48(5)	924.6	0.0	$\frac{7}{2}^-$	$\mapsto$	$\frac{5}{2}^-$
943.4	217(40)	1.10(7)	4234.0	3290.9	$\frac{21}{2}^-$	$\mapsto$	$\frac{17}{2}^-$
969.9	80(10)	1.80(33)*	4233.2	3263.1	$\frac{19}{2}^-$	$\mapsto$	$\frac{15}{2}^-$
996.0	351(70)	0.85(10)	3917.2	2921.2	$\frac{19}{2}^-$	$\mapsto$	$\frac{15}{2}^-$
1035.9	26(5)		4774.8	3739.0	$\frac{21}{2}^-$	$\mapsto$	$\frac{17}{2}^-$
1075.4	393(50)	1.03(6)	2470.3	1394.9	$\frac{13}{2}^-$	$\mapsto$	$\frac{9}{2}^-$
1097.8	76(20)	1.45(16)*	1245.5	147.7	$\frac{5}{2}^-$	$\mapsto$	$\frac{3}{2}^-$
1126.0	28(6)		5359.4	4774.8	$\frac{23}{2}^-$	$\mapsto$	$\frac{19}{2}^-$
1137.5	187(20)	1.01(7)	5371.5	4234.0	$\frac{25}{2}^-$	$\mapsto$	$\frac{21}{2}^-$
1156.9	86(15)		5074.1	3917.2	$\frac{23}{2}^-$	$\mapsto$	$\frac{19}{2}^-$
1186.4	82(20)	0.90(13)	2111.0	924.6	$\frac{11}{2}^-$	$\mapsto$	$\frac{7}{2}^-$
1301.4	135(30)	1.03(13)	6672.9	5371.5	$\frac{29}{2}^-$	$\mapsto$	$\frac{25}{2}^-$
1394.9	315(40)	1.03(7)	1394.9	0.0	$\frac{9}{2}^-$	$\mapsto$	$\frac{5}{2}^-$
1442.0	63(15)	1.37(18)	8114.9	6672.9	$\frac{33}{2}^-$	$\mapsto$	$\frac{29}{2}^-$
1570.0	30(7)		9684.9	8114.9	$\frac{37}{2}^-$	$\mapsto$	$\frac{33}{2}^-$
1581.5	14(4)		1729.0	147.7	$\frac{7}{2}^-$	$\mapsto$	$\frac{3}{2}^-$
1729.0	43(15)	2.05(38)*	1729.0	0.0	$\frac{7}{2}^-$	$\mapsto$	$\frac{5}{2}^-$
1759.0	<17		1759.4	0.0	$\frac{7}{2}^-$	$\mapsto$	$\frac{5}{2}^-$

[a]Uncertainties on the γ-ray energies vary from 0.2 to 0.4 keV for the strong transitions and from 0.8 to 1.0 keV for the weakest ones.
[b]Intensities relative to the intensity of the 714.0-keV transition [2] derived from coincidence gates.
[c]Uncertainties on the excitation energies vary from 0.2 to 0.8 keV.

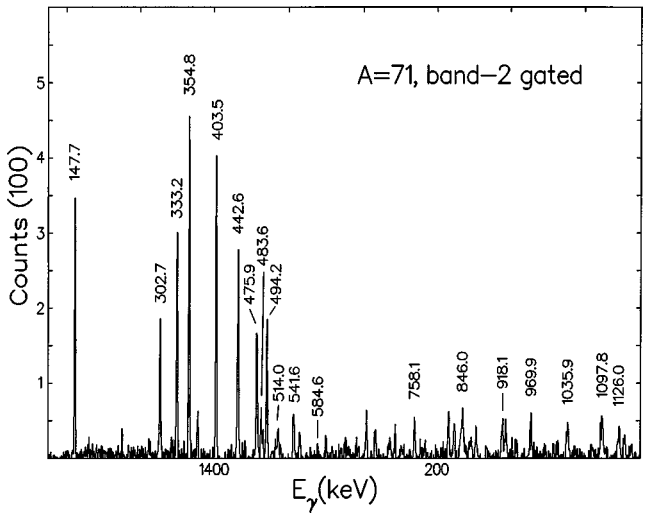

FIG. 2. Spectrum obtained from the sum of coincidence gates placed on the 147.7-, 333.2-, 354.8-, 403.5, 442.6-, 475.9-, and 494.2-keV transitions of band 2 in a matrix gated on $A=71$.

trace of a band crossing within the sequence. TRS calculations [2] for ^{71}As suggest a deformed, prolate shape ($\epsilon_2 \sim 0.31, \gamma \sim 5°$) at $\hbar\omega \sim 0.3$–0.5 MeV, which evolves to a triaxial ($\epsilon_2 \sim 0.24, \gamma \sim 30°$) shape for this negative-parity configuration at high frequencies.

In Fig. 3 the kinematic and dynamic moments of inertia for band 2 are also displayed. Similar behavior to that of band 1 is observed, suggesting similar, prolate deformations. However, band 2 is a $\Delta I=1$ sequence with $B(M1)/B(E2)$ ratios varying between 4 and 6 $\mu_N^2/(e\mathrm{b})^2$. This observation supports a high-K, prolate character for this band. The relevant Nilsson model orbitals [8] as a function of deformation ϵ_2 are shown in Fig. 4. The only available high-K orbital is the $f_{7/2}$ extruder configuration, with asymptotic quantum numbers $7/2^-[303]$, which approaches the Fermi surface at $Z=33$ only for large, $\epsilon_2 > 0.25$, deformations. Although the $5/2^-[303]$ orbital is near the Fermi surface for oblate deformations, $g_K \approx g_R$ for this $f_{5/2}$ orbital. Therefore, the $B(M1)$ value would be very small, in contrast to the observed, relatively large, $B(M1)/B(E2)$ ratios.

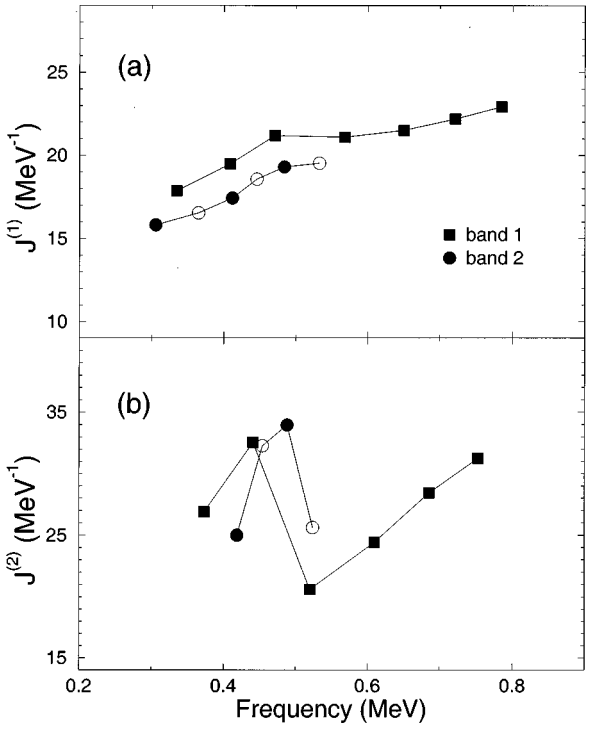

FIG. 3. Kinematic $J^{(1)}$ and dynamic $J^{(2)}$ moments of inertia as a function of rotational frequency (in MeV) for bands 1 (squares) and 2 (circles) in ^{71}As.

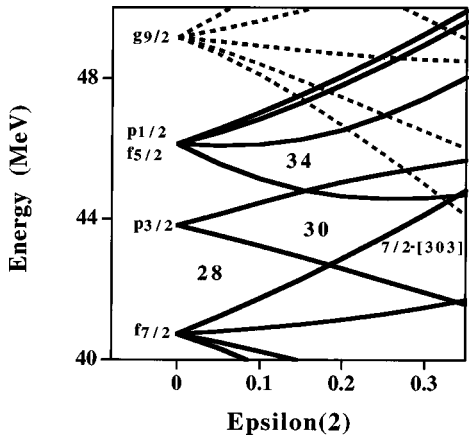

FIG. 4. Nilsson model calculations as a function of deformation ϵ_2 for proton orbitals in ^{71}As. The Nilsson parameters $\kappa=0.0626$ and $\mu=0.614$ were used.

The experimental $B(M1)/B(E2)$ ratios for band 2 are shown in Fig. 5, together with theoretical expectations of this ratio for a $f_{7/2}$, $K=7/2$ proton orbital, with $g_s = 0.65 g_s^{(\mathrm{free})}$ [9]. The $B(E2)$ value for the $17/2^-$ state of band 2 was assumed to be between 58 and 83 W.u., in accordance with experimental limits [2] for the $B(E2)$ value of 68^{+15}_{-10} W.u. for the $17/2^-$ state of band 1. Since both negative-parity

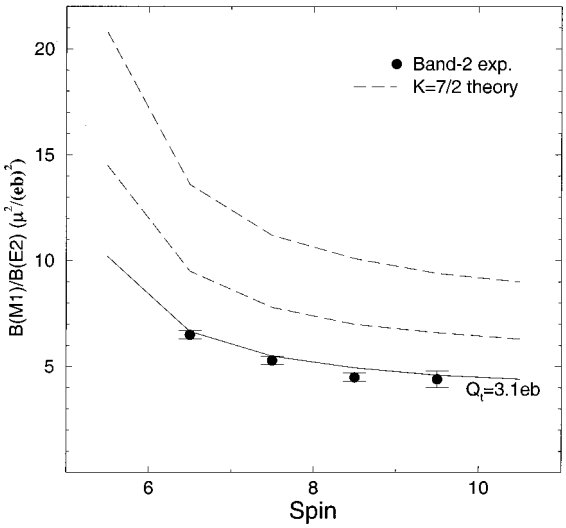

FIG. 5. Experimental $B(M1)/B(E2)$ ratios (circles) for the levels of band 2 as a function of spin. The dashed curves represent the range of values for these ratios expected for the $7/2^-[303]$ proton extruder orbital with empirical $B(E2)$ values for band 1 [2]. The solid curve is expected for moment $Q_t=3.1\ e$b, as discussed in the text.

bands exhibit similar collectivity, this range of values should be a good estimate of the $B(E2)$ value for the $17/2^-$ state of band 2. These theoretical predictions give values somewhat larger than experimentally observed. This could, perhaps, be attributed to a slightly larger prolate deformation in band 2 compared to that measured for band 1. Alternatively, the lack of signature splitting for band 2 suggests an axial shape, up to the highest observed frequency. This could, in turn, correspond to a larger transition quadrupole moment, Q_t, for the same deformation. The experimental $B(M1)/B(E2)$ ratios in Fig. 5 can be reproduced with a moment $Q_t = 3.1\ e$b, which corresponds to an ϵ_2 value of 0.37, using Eq. (3) of Ref. [2].

Proton $7/2^-$ states with modest spectroscopic factors have been previously observed in $(d,{}^3\mathrm{He})$ reactions [10,11] at excitation energies similar to the $7/2^-$ states at the beginning of band 2. However, this is the first clear observation of a deformed rotational band built upon the high-K $7/2^-[303]$ extruder configuration.

In summary, the negative-parity level scheme of ^{71}As has been enriched and extended to higher excitations. The previously known negative-parity triaxial band is extended up to 0.8 MeV rotational frequency. A new $\Delta I = 1$ band is observed with the properties expected for a rotational band built on the $f_{7/2}$, $7/2^-[303]$ proton extruder orbital. This is the first observation of a deformed proton $f_{7/2}$ configuration in the $A = 70$ mass region.

The authors would like to thank Professor Larry Zamick for discussions of the theoretical expectations of the $B(M1)/B(E2)$ ratios. This work was supported in part by U.S. National Science Foundation and the Department of Energy–Nuclear Physics Division under Contract Nos. W-31-109-ENG-38 and DE-AC03-76SF00098.

[1] J.H. Hamilton, A.V. Ramayya, W.T. Pinkston, R.M. Ronningen, G. García Bermúdez, H.K. Carter, R.L. Robinson, H.J. Kim, and R.O. Sayer, Phys. Rev. Lett. **32**, 239 (1974).

[2] R.S. Zighelboim, S.G. Buccino, F.E. Durham, J. Döring, P.D. Cottle, J.W. Holcomb, T.D. Johnson, S.L. Tabor, and P.C. Womble, Phys. Rev. C **50**, 716 (1994).

[3] W. Nazarewicz, J. Dudek, R. Bengtsson, T. Bengtsson, and I. Ragnarsson, Nucl. Phys. **A435**, 397 (1985).

[4] C. Svensson *et al.*, Phys. Rev. Lett. **79**, 1233 (1997); *ibid.* **80**, 2558 (1998).

[5] I.Y. Lee *et al.*, Nucl. Phys. **A520**, 641c (1990).

[6] C.N. Davids *et al.*, Nucl. Instrum. Methods Phys. Res. B **70**, 358 (1992).

[7] N. Fotiades *et al.*, in *ENAM 98*, edited by B. M. Sherrill, D. J. Morrissey, and C. N. Davids, AIP Conf. Proc. No. 455 (AIP, Woodbury, NY, 1998), p. 506; N. Fotiades *et al.*, Bull. Am. Phys. Soc. **43**, 1571 (1998).

[8] B.S. Nilsson, code DIET (unpublished).

[9] A. Bohr and B. Mottelson, *Nuclear Structure* (Benjamin, Reading, MA, 1975), Vol. II, p. 303.

[10] G. Rotbard, G. LaRana, M. Vergnes, G. Berrier, J. Kalifa, F. Guilbault, and R. Tamisier, Phys. Rev. C **18**, 86 (1978).

[11] G. Rotbard, M. Vergnes, J. Vernotte, G. Berrier-Ronsin, J. Kalifa, and R. Tamisier, Nucl. Phys. **A401**, 41 (1983).